HHS Public Access

Author manuscript

J Cancer Res Ther (Manch). Author manuscript; available in PMC 2017 May 24.

Published in final edited form as:

J Cancer Res Ther (Manch). 2013 June ; 1(4): 128–137. doi:10.14312/2052-4994.2013-20.

Development of novel approach to diagnostic imaging of lung cancer with ^{18}F-Nifene PET/CT using A/J mice treated with NNK

V Galitovskiy[1], **SA Kuruvilla**[2], **E Sevriokov**[2], **A Corches**[2], **ML Pan**[2], **M Kalantari-Dehaghi**[1], **AI Chernyavsky**[1], **J Mukherjee**[2,3,*], and **SA Grando**[1,3,*]

[1]Department of Dermatology, University of California-Irvine, Irvine, CA 92697, USA

[2]Preclinical Imaging, Department of Radiological Sciences, University of California-Irvine, Irvine, CA 92697, USA

[3]Cancer Center and Research Institute, University of California-Irvine, Irvine, CA 92697, USA

Abstract

Development of novel methods of early diagnosis of lung cancer is one of the major tasks of contemporary clinical and experimental oncology. In this study, we utilized the tobacco nitrosamine 4-(methylnitrosamino)-1-(3-pyridyl)-1-butanone (NNK)-induced lung cancer in A/J mice as an animal model for development of a new imaging technique for early diagnosis of lung cancer. Lung cancer cells in A/J mice overexpress nicotinic acetylcholine receptors. Longitudinal CT scans were carried out over a period of 8 months after NNK treatment, followed by PET/CT scans with ^{18}F-Nifene that binds to α4-made nicotinic receptors with high affinity. PET/CT scans of lungs were also obtained *ex vivo.* CT revealed the presence of lung nodules in 8-month NNK-treated mice, while control mice had no tumors. Imaging of live animals prior to necropsy allowed correlation of results of tumor load *via* PET/CT and histopathological findings. Significant amount of ^{18}F-Nifene was seen in the lungs of NNK-treated mice, whereas lungs of control mice showed only minor uptake of ^{18}F-Nifene. Quantitative analysis of the extent and amount of ^{18}F-Nifene binding in lung *in vivo* and *ex vivo* demonstrated a higher tumor/nontumor ratio due to selective labeling of tumor nodules expressing abundant α4 nicotinic receptor subunits. For comparison, we performed PET/CT studies with ^{18}F-FDG, which is used for the imaging diagnosis of lung cancer. The tumor/nontumor ratios for ^{18}F-FDG were lower than for ^{18}F-Nifene. Thus, we have developed a novel diagnostic imaging approach to early diagnosis of lung cancer using ^{18}F-Nifene PET/CT. This technique allows quantitative assessment of lung tumors in live mice, which is critical for establishing tumor size and location, and also has salient clinical implications.

[*]Corresponding authors: Grando SA, 134 Sprague Hall, University of California-Irvine, Irvine, CA 92697, USA. Tel.: 949-824-2713; Fax: 949824-2993, sgrando@uci.edu; and Mukherjee J, B138 Medical Sciences, University of California-Irvine, Irvine, CA 92697, USA. Tel.: 949-824-2018; Fax: 949-824-2344, j.mukherjee@uci.edu.

[*]Both senior authors contributed equally to this paper.

Conflict of interest

All the authors declare that they have no conflict of interest.

Keywords

^{18}F-Nifene; ^{18}F-FDG; PET/CT imaging; nicotinic receptors; NNK; A/J mice; lung cancer

Introduction

Lung cancer is the leading cause of cancer death in industrialized countries with a high mortality rate and 5-year survival rates of <15% [1]. Early detection of lung cancer is essential for early therapeutic interventions which can reduce mortality. Minimally invasive methods for early detection of lung cancer include computerized tomography (CT) and positron emission tomography (PET). A combination of PET/CT has been shown to have a higher sensitivity of detection of the primary tumor and metastases and also correlates with pathology [2]. The ^{18}F-fluorodeoxyglucose (^{18}F-FDG) PET/CT is being used for detection of the primary lung tumor and metastases. However, there is still a substantial need for improving sensitivity and specificity of PET/CT lung cancer detection than is currently possible [3]. This goal can be achieved by using more specific probes.

Acetylcholine (ACh) is an auto/paracrine growth factor for lung cancer [4]. Recent studies have demonstrated that the nicotinic class ACh receptors (nAChRs) act as central mediators in the cancer signaling pathways, and have unveiled previously unknown nicotinergic signaling networks in the lung (reviewed in [5–7]). nAChRs are classic representatives of the superfamily of ligand-gated ion channel proteins mediating the influx of Na^+ and Ca^{2+} and efflux of K^+ [8]. The subunit genes encoding a pentameric protein have been identified and designated α1-α10, β1-β4, ε, δ, and γ. Although expression of nAChRs was originally thought to be limited to neurons and skeletal muscles, contemporary research has convincingly demonstrated expression of different combinations of the “neuronal” nAChR subunits α2-α10 and β2-β4 in practically all cell types [9]. Activation of nAChRs modulates expression of a diverse set of proteins, including the nAChRs themselves [10–16], which can contribute to the carcinogenic action of tobacco constituents [10, 17–19]. The nAChR subtypes in lung epithelial cells are well-characterized. In 1997, we first demonstrated that human bronchial cells express the α3, α4, α5, and α7 subunits that form nAChR channels modulating Ca^{2+} metabolism [20]. These findings have been confirmed in other laboratories [21–23].

Tobacco-specific nitrosamines, N′-nitrosonornicotine and 4-(methylnitrosamino)-1-(3-pyridyl)-1-butanone (NNK) (Figure 1), are nicotine metabolites and powerful lung carcinogens that bind to nAChRs [24, 25]. Exposure to nicotine or NNK activates and upregulates respiratory nAChRs [10, 16, 19, 20, 26, 27]. Bronchial cell transformation also alters the expression of nAChR subunit profiles [4, 23, 28]. The nAChR subtypes are overexpressed in a variety of cancers, including lung cancer [6, 7, 29]. Hence, development of novel and more sensitive methods of early diagnosis of lung cancer may be based on visualizing nAChRs on cancer cells. However, there have been no reports on *in vivo* visualization of lung cancer using the nAChR imaging probes.

We have developed and validated an imaging probe, ^{18}F-Nifene (Figure 1), which is suitable for non-invasive visualization of $\alpha4\beta2$ nAChRs using PET [30–32]. Normal lung

distribution and kinetics of ^{18}F-Nifene in mice was characterized by us in a previous work [33]. Binding of ^{18}F-Nifene in rat brain correlates very well with the known distribution of $\alpha4\beta2$ receptors, as defined by ^{125}I-iodoepibatidine [30, 34, 35] and confirmed in the studies with $\beta2$-knockout mice (36). The goal of this study was to evaluate utility of ^{18}F-Nifene as an imaging probe in the early diagnosis of lung cancer. Since ^{18}F-FDG PET/CT is routinely used for diagnosis of human lung tumors [2], comparative PET/CT studies were also carried out with ^{18}F-FDG.

As an animal model of lung cancer, we chose A/J mice treated with NNK. This model has been employed by us in previous studies [37, 38]. The time between exposure to a carcinogen and appearance of multiple tumor nodules in the lungs is relatively short: 4 to 5 months [39]. The tumors display a histological pattern characteristic of alveolobronchial adenomas and alveolobronchial adenocarcinomas [40, 41] resembling the human lung adenocarcinoma that has increased in incidence in the United States [42]. Mouse tumors originate from the same cells—the type II alveolar epithelial cells and Clara cells. The lung adenocarcinoma developing in A/J mice exposed to tobacco products is associated with overexpression of nAChRs and relies on nAChR signaling [10, 19].

Herein, we report the use of ^{18}F-Nifene in the longitudinal PET/CT studies of lung tumors in A/J mice treated with NNK. These tumors were found to overexpress the $\alpha4$-made nAChRs providing the tumor-selective and specific target for ^{18}F-Nifene. The results demonstrated that our newly developed ^{18}F-Nifene PET/CT method allows quantitative assessment of lung tumors in live mice, which is critical for establishing tumor size and location, and has salient clinical implications.

Materials and methods

A/J mouse model of lung cancer

Female strain A/J mice, 6–8 weeks old, were purchased from Jackson Laboratories (Bar Harbor, ME). Mice of this strain develop lung tumors when exposed to tobacco nitrosamines [43]. The animals were housed in polypropylene boxes with *ad libitum* access to food and water, and conventional bedding material. Mice were treated in accordance to National Institutes of Health guidelines and as approved by the Institutional Animal Care and Use Committee of the University of California, Irvine. Mice were divided into three groups, 12 per group (Figure 2). Experimental mice were treated with NNK by subcutaneous injection of 100 μl in the upper back at a dose of 100 mg/kg once a week for four weeks. NNK was dissolved in DMSO in 10× concentration and diluted in corn oil to final concentration. Treatment control mice were injected with the same solution without NNK. The CT/PET control mice were also included because multiple CT scans might induce lung cancer in A/J mice. Lung tissue sections from control and NNK-treated A/J mice were obtained following PET/CT scans (after a 24-hr period once the fluorine-18 radioactivity had decayed away) and stained with hematoxylin and eosin. Using rabbit polyclonal antibody to $\alpha4$ nAChR subunit (Millipore, Temecula, CA), the $\alpha4$-containing nAChR subtypes were visualized by immunofluorescence in the cryostat sections of lung tissue, and also by immunoblotting of lung homogenates. Protein bands were visualized by affinity purified goat anti-rabbit secondary antibody conjugated to IRDye 680 or IRDye800 (Rockland, Inc., Gilbertsville,

PA). Fluorescent signal was detected by scanning the nitrocellulose filter in a LI-COR Odyssey near infrared imaging platform and quantified using Odyssey 2.1 software (LI-COR Biotechnology, Lincoln, NE). Visualization of α-tubulin with a respective antibody from Millipore was used as a loading control.

Radiochemicals

Synthesis of ^{18}F-Nifene has been established and was carried out following reported procedures [32]. The automated radiosynthesis of ^{18}F-Nifene was carried out in the CPCU (chemistry-processing control unit) box. An Alltech C column (10 μm, 250 × 10 mm^2) was used for reverse-phase HPLC purification. Specific activity of ^{18}F-Nifene was approximately 2000 Ci/mmol. The collected fraction was taken to near dryness in vacuo. The final formulation of ^{18}F-Nifene was carried out using approximately 2 to 5 mL of 0.9% saline followed by filtration through a membrane filter (0.22 μm) into a sterile dose vial for use in the PET studies. ^{18}F-FDG was purchased from PETNET solutions (Irvine, CA). Fluorine-18 radioactivity was counted in a Capintec CRC-15R dose calibrator, while low level counting was carried out in a Capintec Caprac-R well-counter.

In vivo CT and PET imaging studies

CT Imaging—Prior to imaging, mice were fasted in a dark quiet place for > 6 hours. In preparation for the scans, mice were anaesthetized with isoflurane and then maintained under anesthesia during the scan (2–4% induction and 2–2.5% maintenance). An Inveon Multimodality (MM) CT scanner (Siemens Medical Solutions, Malvern, PA), which has a resolution of 1.46 mm in the center of the field-of-view, was used for CT acquisitions in combined PET/CT experiments [44]. Abdominal images of the mice were obtained with a large area detector (4096 × 4096 pixels, 10 cm × 10 cm field-of-view). The CT projections were acquired with the detector-source assembly rotating over 360 degrees and 720 rotation steps. A projection bin factor of 4 was used in order to increase the signal to noise ratio in the images. The CT images were reconstructed using cone-beam reconstruction with a Shepp filter with cutoff at Nyquist frequency resulting in an image matrix of 480 × 480 × 632 and a voxel size of 0.206 mm. Longitudinal CT studies were analyzed using Inveon Research Workplace (IRW, Siemens Medical Solutions, Malvern, PA), software. Volumes of interest (3D VOIs) were drawn manually on the lungs of control and NNK-treated mice. VOIs were drawn as irregular contours on the high resolution CT images, and tumor volumes at different time intervals (baseline to 10 months) of the same mice were calculated by using the segmentation function in the IRW software.

^{18}F-Nifene and ^{18}F-FDG PET imaging—Mice were injected with 100 μCi ^{18}F-Nifene or 100 μCi ^{18}F-FDG via tail vein under anesthesia. The animals were then placed in the mouse chamber and were positioned in the Inveon Multimodality CT/PET scanner. The Inveon PET/CT was switched to the “docked mode” for combined PET/CT experiments. A CT scan was then obtained for reconstruction of the PET data and further analysis of the PET/CT data. Duration of the PET scan was typically 30 min and was timed to start 60 min post injection of ^{18}F-Nifene or ^{18}F-FDG. The images were reconstructed using fourier rebinning and 2-dimensional filtered back-projection (2D FBP) method (ramp filter and cutoff at Nyquist frequency) with an image matrix of 128×128×159, resulting in a pixel size

of 0.77 mm and a slice thickness of 0.796 mm. The PET data for both ^{18}F-Nifene and ^{18}F-FDG were analyzed as tumor to nontumor ratios. Similar to previously described methods (45), the VOIs were first delineated visually by contouring the ^{18}F-Nifene or ^{18}F-FDG activity that was clearly above normal background activity in the lungs. These areas were confirmed in the corresponding CT of each animal. The amount of ^{18}F-Nifene or ^{18}F-FDG activity in each VOI (in kBq/mL) of the tumor and areas of the lung that did not have any tumors were measured and confirmed using the corresponding CT scans of each individual animal.

Ex vivo PET/CT studies

Mice were decapitated after an ^{18}F-Nifene or an ^{18}F-FDG scan, and the lungs were rapidly removed and frozen. The whole lungs from control mice and NNK-treated mice were placed in a hexagonal polystyrene weighing boat (top edge side length 4.5 cm, bottom edge side length 3 cm) and covered with powdered dry ice. This boat was placed securely on the scanner bed. PET and CT scans were acquired simultaneously of the control and NNK-treated mice lungs for 30 min. Images were analyzed using the Acquisition Sinogram Image Processing (ASIPRO, Siemens Medical Solutions, Malvern, PA) and IRW software from Siemens Medical Solutions.

Results

In vivo ^{18}F-Nifene PET/CT studies

The longitudinal CT image analysis of the scans showed absence of tumors in control mice and multiple tumors in both lungs of all NNK-treated animals (Figure 3). The rate of growth of the tumors increased significantly after the 6th month post-NNK treatment (Table 1). Figure 4 shows the distribution of ^{18}F-Nifene in a control and NNK-treated A/J mice. The urinary bladder ^{18}F-Nifene uptake increased over time, while the liver and kidneys retained a significant amount of radioactivity. This distribution of ^{18}F-Nifene in the lungs of control A/J mice was similar to that previously seen in BALB/c mice [33], demonstrating that normal lungs have very low ^{18}F-Nifene uptake. In contrast to control A/J mice, NNK-treated animals exhibited a significant amount of ^{18}F-Nifene uptake and binding in the lungs. Volume of lung tumors correlated directly with time interval after NNK treatment, showing a rapid increase after 6 months when the tumor volume exceeded 7 mm^3 (Figure 3C). Multiple lung tumor nodules retaining ^{18}F-Nifene were confirmed by the coregistered PET/CT images (Figure 4). Quantitative analysis of the extent and amount of ^{18}F-Nifene binding provided tumor/nontumor ratios of 1.8–2.0.

Ex vivo studies of lung ^{18}F-Nifene uptake

In order to ascertain the difference in ^{18}F-Nifene uptake in the control *vs.* NNK-treated mice, the lungs were excised after the *in vivo* studies. *Ex vivo* studies of the control A/J mice lungs showed very little binding of ^{18}F-Nifene (Figure 5). The lungs from A/J mice treated with NNK demonstrated significantly higher ^{18}F-Nifene binding, which was predominantly localized to the tumor nodules (Figure 5C). Quantitative analysis of the extent and amount of ^{18}F-Nifene binding provided the tumor/nontumor ratios > 4.

Comparative ^{18}F-Nifene and ^{18}F-FDG studies

We compared efficacy of ^{18}F-Nifene and ^{18}F-FDG for early diagnosis of lung tumor in A/J mice. ^{18}F-FDG PET/CT is an established approach to imaging diagnosis of lung cancer [2]. Uptake of ^{18}F-FDG in the fasted control mice occurred in the brain with low amounts in the heart and other peripheral organs (Figure 6). Greater brown adipose tissue uptake of ^{18}F-FDG in NNK-treated mice was in keeping with the reports on the effects of nicotine on this tissue (46). While ^{18}F-Nifene was excreted into the kidney and urinary bladder, ^{18}F-Nifene was also retained in the brain, particularly in the nAChR-rich thalamus [36]. Control mice showed little uptake of ^{18}F-FDG in the lung, which was in agreement with the ^{18}F-FDG PET/CT scan (Figure 7A–D). The NNK-treated animals clearly exhibited the presence of multiple tumor nodules in the lungs in the *in vivo* CT (Figure 7E). Uptake of ^{18}F-FDG was seen in these regions (Figure 7F) and was confirmed in the PET/CT coregistered image in Figure 7G. The uptake in the heart made it difficult to clearly visualize some of the tumor nodules. However, when the lung was excised from the NNK-treated mice, the *ex vivo* scan localized the ^{18}F-FDG uptake to lung tumors (Figure 7H). The tumor-localized ^{18}F-FDG uptake was not present in the lungs of control animals.

Overexpression of α4 nAChR in lung tumors of A/J mice

Immunoblots of lung proteins from tumor-free control A/J mouse vs. tumor-free and tumor-containing lungs of mice treated with NNK demonstrated overexpression of $\alpha 4$ nAChR subunit in the tumor-containing lung (Figure 8A). Immunofluorescence staining of lung sections of the control (not shown) and NNK-treated A/J mice showed preferential binding of $\alpha 4$ antibody to cancer cells comprising the tumor loci visualized by light microscopy (Figure 8B,C). These results confirmed that the lung tumor nodules retaining ^{18}F-Nifene expressed large amounts of $\alpha 4$-made nAChRs.

Discussion

This study was focused on development and validation of the PET/CT diagnostic imaging methodology utilizing ^{18}F-Nifene. Previous works have established that ^{18}F-Nifene is a highly specific radioligand of $\alpha 4\beta 2$ nAChR [30–32, 34–36]. Herein, we tested the hypothesis that ^{18}F-Nifene can visualize $\alpha 4$-made nAChRs in the lung tumors of NNK-treated A/J mice, thus enabling early diagnosis of lung cancer. Imaging of live animals prior to necropsy allowed correlation of the tumor load identified by PET/CT and histopathology. The obtained results demonstrated for the first time feasibility to visualize lung cancer lesions in live A/J mice, and quantitatively characterize lung tumor load starting from the very beginning of tumor development.

Our findings vividly demonstrated that lung cancer cells in A/J mice abundantly express the $\alpha 4$ subunit-containing nAChRs binding ^{18}F-Nifene. This was illustrated by immunoblotting and corroborated by immunohistochemical studies with specific anti-$\alpha 4$ antibody, and is also in keeping with previous reports of upregulated $\alpha 4$ expression in nicotine-treated lung cancer cells [26, 47, 48]. Furthermore, it has been reported that NNK upregulates $\alpha 4$ nAChR [49]. While previous studies of smoker's lungs as well as human and monkey bronchial cells exposed to nicotine also demonstrated overexpression of $\alpha 7$ nAChR [16, 20], the analysis of

transcriptomes of tumor-containing lungs from the A/J mice treated with NNK did not confirm overexpression of the $\alpha 7$ subunit gene [37]. Therefore, $\alpha 4$ nAChR subunit appears to be a specific marker of NNK-induced lung tumors in the A/J mouse strain.

It has been demonstrated that activation of nAChRs on respiratory cells can contribute directly to lung tumorigenesis [50, 51]. Activation of nAChRs stimulates the growth of lung cancer cells, in part, through $\alpha 4$ nAChR and suppresses apoptosis [23, 52–58], indicating that nicotine can act as a tumor promoter that facilitates the outgrowth of cells with genetic damage. In addition to a well-formulated etiologic role of tobacco nitrosamines in the genotoxic damage inducing lung cancer, recent studies have identified tobacco nitrosamines as high-affinity agonists of nAChRs that can upregulate cell growth [59]. Therefore, it is currently believed that pulmonary nAChRs act as central mediators in the activation of cancer signaling pathways [60], and these receptors are considered as novel drug targets for prevention and treatment of lung cancer [61–64].

The ability of ^{18}F-Nifene to detect NNK-induced lung cancer in A/J mice was evident, compared to the very low retentions of ^{18}F-Nifene in lungs of control mice. Postmortem histopathological analysis of the lungs confirmed the presence of tumors. No significant difference in brain ^{18}F-Nifene binding was observed between control and NNK-treated mice. The whole-body distribution of ^{18}F-Nifene in intact mice has been recently described by us elsewhere [33]. Since uptake of ^{18}F-Nifene in the heart is low, delineation of lung tumor uptake was not hampered from spillover of activity from the heart. The tumor/nontumor ratios were approximately 2, illustrating greater ^{18}F-Nifene binding to the tumors. An increased lung tumor uptake of ^{18}F-Nifene was confirmed by *ex vivo* studies of the excised lungs, showing the tumor/nontumor ratios >4. Although the *ex vivo* CT of the lungs from NNK-treated mice revealed large amounts of tumor nodules, *in vivo* CT was not as clearly discernible. This fact indicates that combining CT with PET increased sensitivity of detection of small lung tumors.

For comparison, we also performed PET/CT studies with ^{18}F-FDG, which is currently clinically used for the imaging diagnosis of lung cancer (2). The tumor to nontumor ratios for ^{18}F-FDG were lower which may be accounted for by the lower ^{18}F-FDG by lung tumors compared to ^{18}F-Nifene. Additionally, a higher background from the considerable uptake of ^{18}F-FDG in heart affected accurate ^{18}F-FDG quantification in the lungs. Thus, the ability of ^{18}F-FDG imaging to detect lung tumors *in vivo* was lower than that of ^{18}F-Nifene.

Conclusion

We have developed a novel diagnostic imaging approach to early diagnosis of lung cancer using ^{18}F-Nifene PET/CT. Results of our experimental studies in the NNK-treated A/J mice as a lung cancer model showed that longitudinal PET/CT studies with ^{18}F-Nifene may be useful. This is a first study employing ^{18}F-Nifene for evaluation of nAChRs in tumor bearing lungs. Although it is premature to assess clinical value of this new imaging agent at this point, further studies are planned in order to demonstrate the imaging diagnostic approach employing ^{18}F-Nifene PET/CT. The ^{18}F-Nifene PET/CT is a relatively short procedure, 30 min, which should be a very useful feature for its clinical usage.

Acknowledgments

This research was supported by the National Institutes of Health grants R01AG029479 (JM) and S10RR024546 (JM) and R01ES017009 (SG) and a research grant from American Lung Association to SG. We thank Drs. Harmadeep Dhaliwal, Cristian Constantinescu and M. Reza Mirbolooki for their invaluable assistance with performing and analyzing certain experiments described in this paper.

References

1. Jemal A, Siegel R, Ward E, Hao Y, Xu J, et al. Cancer statistics, 2008. CA Cancer J Clin. 2008; 58:71–96. [PubMed: 18287387]
2. Cheebsumon P, Boellaard R, de Ruysscher D, van Elmpt W, van Baardwijk A, et al. Assessment of tumour size in PET/CT lung cancer studies: PET-and CT-based methods compared to pathology. EJNMMI Res. 2012; 2:56. [PubMed: 23034289]
3. Navani N, Spiro SG. PET scanning is important in lung cancer; but it has its limitations. Respirology. 2010; 15:1149–1151. [PubMed: 20920122]
4. Song P, Spindel ER. Basic and clinical aspects of non-neuronal acetylcholine: expression of non-neuronal acetylcholine in lung cancer provides a new target for cancer therapy. J Pharmacol Sci. 2008; 106:180–185. [PubMed: 18285655]
5. Improgo MR, Tapper AR, Gardner PD. Nicotinic acetylcholine receptor-mediated mechanisms in lung cancer. Biochem Pharmacol. 2011; 82:1015–1021. [PubMed: 21640716]
6. Singh S, Pillai S, Chellappan S. Nicotinic acetylcholine receptor signaling in tumor growth and metastasis. J Oncol. 2011; 2011:456743. [PubMed: 21541211]
7. Schuller HM. Regulatory role of the $\alpha 7$ nAChR in cancer. Curr Drug Targets. 2012; 13:680–687. [PubMed: 22300035]
8. Steinbach, JH. Mechanism of action of the nicotinic acetylcholine receptor. In: Bock, G., Marsh, J., editors. The Biology Of Nicotine Dependence. Meeting; London, England, UK: New York: John Wiley and Sons Ltd; 1990. p. 53-61.November 7–9 1989
9. Grando SA, Kawashima K, Kirkpatrick CJ, Meurs H, Wessler I. The non-neuronal cholinergic system: basic science, therapeutic implications and new perspectives. Life Sci. 2012; 91:969–972.
10. Davis R, Rizwani W, Banerjee S, Kovacs M, Haura E, et al. Nicotine promotes tumor growth and metastasis in mouse models of lung cancer. PLoS One. 2009; 4:e7524. [PubMed: 19841737]
11. Dunckley T, Lukas RJ. Nicotine modulates the expression of a diverse set of genes in the neuronal SH-SY5Y cell line. J Biol Chem. 2003; 278:15633–15640. [PubMed: 12588870]
12. Sekhon HS, Jia Y, Raab R, Kuryatov A, Pankow JF, et al. Prenatal nicotine increases pulmonary alpha7 nicotinic receptor expression and alters fetal lung development in monkeys. J Clin Invest. 1999; 103:637–647. [PubMed: 10074480]
13. Arredondo J, Nguyen VT, Chernyavsky AI, Jolkovsky DL, Pinkerton KE, et al. A receptor-mediated mechanism of nicotine toxicity in oral keratinocytes. Lab Invest. 2001; 81:1653–1668. [PubMed: 11742036]
14. Arredondo J, Chernyavsky AI, Jolkovsky DL, Pinkerton KE, Grando SA. Receptor-mediated tobacco toxicity: acceleration of sequential expression of alpha5 and alpha7 nicotinic receptor subunits in oral keratinocytes exposed to cigarette smoke. FASEB J. 2008; 22:1356–1368. [PubMed: 18450646]
15. Arredondo J, Chernyavsky AI, Marubio LM, Beaudet AL, Jolkovsky DL, et al. Receptor-mediated tobacco toxicity: regulation of gene expression through alpha3beta2 nicotinic receptor in oral epithelial cells. Am J Pathol. 2005; 166:597–613. [PubMed: 15681842]
16. Fu XW, Lindstrom J, Spindel ER. Nicotine activates and upregulates nicotinic acetylcholine receptors in bronchial epithelial cells. Am J Respir Cell Mol Biol. 2009; 41:93–99. [PubMed: 19097990]
17. Wong HP, Yu L, Lam EK, Tai EK, Wu WK, et al. Nicotine promotes cell proliferation via alpha7-nicotinic acetylcholine receptor and catecholamine-synthesizing enzymes-mediated pathway in human colon adenocarcinoma HT-29 cells. Toxicol Appl Pharmacol. 2007; 221:261–267. [PubMed: 17498763]

18. Plummer HK 3rd, Dhar M, Schuller HM. Expression of the alpha7 nicotinic acetylcholine receptor in human lung cells. Respir Res. 2005; 6:29. [PubMed: 15807899]
19. Razani-Boroujerdi S, Sopori ML. Early manifestations of NNK-induced lung cancer: role of lung immunity in tumor susceptibility. Am J Respir Cell Mol Biol. 2007; 36:13–19. [PubMed: 16873770]
20. Zia S, Ndoye A, Nguyen VT, Grando SA. Nicotine enhances expression of the alpha 3, alpha 4, alpha 5, and alpha 7 nicotinic receptors modulating calcium metabolism and regulating adhesion and motility of respiratory epithelial cells. Res Res Commun Mol Pathol Pharmacol. 1997; 97:243–262. [PubMed: 9387186]
21. Maus AD, Pereira EF, Karachunski PI, Horton RM, Navaneetham D, et al. Human and rodent bronchial epithelial cells express functional nicotinic acetylcholine receptors. Mol Pharmacol. 1998; 54:779–788. [PubMed: 9804613]
22. Proskocil BJ, Sekhon HS, Jia Y, Savchenko V, Blakely RD, et al. Acetylcholine is an autocrine or paracrine hormone synthesized and secreted by airway bronchial epithelial cells. Endocrinology. 2004; 145:2498–2506. [PubMed: 14764638]
23. West KA, Brognard J, Clark AS, Linnoila IR, Yang X, et al. Rapid Akt activation by nicotine and a tobacco carcinogen modulates the phenotype of normal human airway epithelial cells. J Clin Invest. 2003; 111:81–90. [PubMed: 12511591]
24. Schuller HM, Orloff M. Tobacco-specific carcinogenic nitrosamines. Ligands for nicotinic acetylcholine receptors in human lung cancer cells. Biochem Pharmacol. 1998; 55:1377–1384. [PubMed: 10076528]
25. El-Bayoumy K, Iatropoulos M, Amin S, Hoffmann D, Wynder EL. Increased expression of cyclooxygenase-2 in rat lung tumors induced by the tobacco-specific nitrosamine4-(methylnitrosamino)-4-(3-pyridyl)-1-butanone: the impact of a high-fat diet. Cancer Res. 1999; 59:1400–1403. [PubMed: 10197601]
26. Lam DC, Girard L, Ramirez R, Chau WS, Suen WS, et al. Expression of nicotinic acetylcholine receptor subunit genes in non-small-cell lung cancer reveals differences between smokers and nonsmokers. Cancer Res. 2007; 67:4638–4647. [PubMed: 17510389]
27. Al-Wadei HA, Al-Wadei MH, Masi T, Schuller HM. Chronic exposure to estrogen and the tobacco carcinogen NNK cooperatively modulates nicotinic receptors in small airway epithelial cells. Lung Cancer. 2010; 69:33–39. [PubMed: 19896235]
28. Carlisle DL, Liu X, Hopkins TM, Swick MC, Dhir R, et al. Nicotine activates cell-signaling pathways through muscle-type and neuronal nicotinic acetylcholine receptors in non-small cell lung cancer cells. Pulm Pharmacol Ther. 2007; 20:629–641. [PubMed: 17015027]
29. Wu CH, Lee CH, Ho YS. Nicotinic acetylcholine receptor-based blockade: applications of molecular targets for cancer therapy. Clin Cancer Res. 2011; 17:3533–3541. [PubMed: 21444681]
30. Kant R, Constantinescu CC, Parekh P, Pandey SK, Pan ML, et al. Evaluation of F-nifene binding to $\alpha 4\beta 2$ nicotinic receptors in the rat brain using microPET imaging. EJNMMI Res. 2011; 1
31. Hillmer AT, Wooten DW, Slesarev MS, Ahlers EO, Barnhart TE, et al. PET imaging of $\alpha 4\beta 2$* nicotinic acetylcholine receptors: quantitative analysis of ^{18}F-nifene kinetics in the nonhuman primate. J Nucl Med. 2012; 53:1471–1480. [PubMed: 22851633]
32. Pichika R, Easwaramoorthy B, Collins D, Christian BT, Shi B, et al. Nicotinic alpha4beta2 receptor imaging agents: part II. Synthesis and biological evaluation of 2-[^{18}F]fluoro-3-[2-((S)-3-pyrrolinyl)methoxy]pyridine (^{18}F-nifene) in rodents and imaging by PET in nonhuman primate. Nucl Med Biol. 2006; 33:295–304. [PubMed: 16631077]
33. Constantinescu CC, Garcia A, Mirbolooki MR, Pan ML, Mukherjee J. Evaluation of [^{18}F]Nifene biodistribution and dosimetry based on whole-body PET imaging of mice. Nucl Med Biol. 2013; 40:289294.
34. Easwaramoorthy B, Pichika R, Collins D, Potkin SG, Leslie FM, et al. Effect of acetylcholinesterase inhibitors on the binding of nicotinic alpha4beta2 receptor PET radiotracer, (18)F-nifene: A measure of acetylcholine competition. Synapse. 2007; 61:29–36. [PubMed: 17068780]

35. Perry DC, Xiao Y, Nguyen HN, Musachio JL, Dávila-García MI, et al. Measuring nicotinic receptors with characteristics of alpha4beta2, alpha3beta2 and alpha3beta4 subtypes in rat tissues by autoradiography. J Neurochem. 2002; 82:468–481. [PubMed: 12153472]
36. Bieszczad KM, Kant R, Constantinescu CC, Pandey SK, Kawai HD, et al. Nicotinic acetylcholine receptors in rat forebrain that bind ^{18}F-nifene: relating PET imaging, autoradiography, and behavior. Synapse. 2012; 66:418–434. [PubMed: 22213342]
37. Gordon W, Galitovskiy V, Edwards R, Andersen B, Grando SA. The tobacco carcinogen nitrosamine induces a differential gene expression response in tumour susceptible A/J and resistant C3H mouse lungs. Eur J Cancer. 2013; 49:725–733. doi:pii: S0959-8049(12)00689-2.10.1016/j.ejca.2012.08.027. [PubMed: 23010150]
38. Galitovskiy V, Chernyavsky AI, Edwards RA, Grando SA. Muscle sarcomas and alopecia in A/J mice chronically treated with nicotine. Life Sci. 2012; 91:1109–1112. [PubMed: 22521759]
39. Witschi H. Successful and not so successful chemoprevention of tobacco smoke-induced lung tumors. Exp Lung Res. 2000; 26:743–755. [PubMed: 11195468]
40. Malkinson AM. Molecular comparison of human and mouse pulmonary adenocarcinomas. Exp Lung Res. 1998; 24:541–555. [PubMed: 9659582]
41. Malkinson AM. Primary lung tumors in mice: an experimentally manipulable model of human adenocarcinoma. Cancer Res. 1992; 52:2670s–2676s. [PubMed: 1562998]
42. Thun MJ, Lally CA, Flannery JT, Calle EE, Flanders WD, et al. Cigarette smoking and changes in the histopathology of lung cancer. J Natl Cancer Inst. 1997; 89:1580–1586. [PubMed: 9362155]
43. Hecht SS, Isaacs S, Trushin N. Lung tumor induction in A/J mice by the tobacco smoke carcinogens 4-(methylnitrosamino)-1-(3-pyridyl)-1-butanone and benzo[a]pyrene: a potentially useful model for evaluation of chemopreventive agents. Carcinogenesis. 1994; 15:2721–2725. [PubMed: 8001227]
44. Constantinescu CC, Mukherjee J. Performance evaluation of an Inveon PET preclinical scanner. Phys Med Biol. 2009; 54:2885–2899. [PubMed: 19384008]
45. Schinagl DA, Span PN, Oyen WJ, Kaanders JH. Can FDG PET predict radiation treatment outcome in head and neck cancer? Results of a prospective study. Eur J Nucl Med Mol Imaging. 2011; 38:1449–1458. [PubMed: 21461734]
46. Baba S, Tatsumi M, Ishimori T, Lilien DL, Engles JM, et al. Effect of nicotine and ephedrine on the accumulation of ^{18}F-FDG in brown adipose tissue. J Nucl Med. 2007; 48:981–986. [PubMed: 17504863]
47. Al-Wadei HA, Al-Wadei MH, Schuller HM. Cooperative regulation of non-small cell lung carcinoma by nicotinic and beta-adrenergic receptors: a novel target for intervention. PLoS One. 2012; 7:e29915. [PubMed: 22253823]
48. Al-Wadei HA, Al-Wadei MH, Ullah MF, Schuller HM. Gamma-amino butyric acid inhibits the nicotine-imposed stimulatory challenge in xenograft models of non-small cell lung carcinoma. Curr Cancer Drug Targets. 2012; 12:97–106. [PubMed: 22165966]
49. Al-Wadei HA, Schuller HM. Nicotinic receptor-associated modulation of stimulatory and inhibitory neurotransmitters in NNK-induced adenocarcinoma of the lungs and pancreas. J Pathol. 2009; 218:437–445. [PubMed: 19274673]
50. Minna JD. Nicotine exposure and bronchial epithelial cell nicotinic acetylcholine receptor expression in the pathogenesis of lung cancer. J Clin Invest. 2003; 111:31–33. [PubMed: 12511585]
51. Paleari L, Grozio A, Cesario A, Russo P. The cholinergic system and cancer. Semin Cancer Biol. 2008; 18:211–217. [PubMed: 18262434]
52. Maneckjee R, Minna JD. Opioid and nicotine receptors affect growth regulation of human lung cancer cell lines. Proc Natl Acad Sci U S A. 1990; 87:3294–3298. [PubMed: 2159143]
53. Maneckjee R, Minna JD. Opioids induce while nicotine suppresses apoptosis in human lung cancer cells. Cell Growth Differ. 1994; 5:1033–1040. [PubMed: 7848904]
54. Schuller HM, Nylen E, Park P, Becker KL. Nicotine, acetylcholine and bombesin are trophic growth factors in neuroendocrine cell lines derived from experimental hamster lung tumors. Life Sci. 1990; 47:571–578. [PubMed: 1698239]

55. Schuller HM, Plummer HK 3rd, Jull BA. Receptor-mediated effects of nicotine and its nitrosated derivative NNK on pulmonary neuroendocrine cells. Anat Rec A Discov Mol Cell Evol Biol. 2003; 270A:51–58.

56. Song P, Sekhon HS, Jia Y, Keller JA, Blusztajn JK, et al. Acetylcholine is synthesized by and acts as an autocrine growth factor for small cell lung carcinoma. Cancer Res. 2003; 63:214–221. [PubMed: 12517800]

57. Cattaneo MG, D'atri F, Vicentini LM. Mechanisms of mitogen-activated protein kinase activation by nicotine in small-cell lung carcinoma cells. Biochem J. 1997; 328:499–503. [PubMed: 9371707]

58. Sun X, Ritzenthaler JD, Zheng Y, Roman J, Han S. Rosiglitazone inhibits alpha4 nicotinic acetylcholine receptor expression in human lung carcinoma cells through peroxisome proliferator-activated receptor gamma-independent signals. Mol Cancer Ther. 2009; 8:110–118. [PubMed: 19139119]

59. Grando SA. Basic and clinical aspects of non-neuronal acetylcholine: biological and clinical significance of non-canonical ligands of epithelial nicotinic acetylcholine receptors. J Pharmacol Sci. 2008; 106:174–179. [PubMed: 18285656]

60. Schuller HM. Is cancer triggered by altered signalling of nicotinic acetylcholine receptors? Nat Rev Cancer. 2009; 9:195–205. [PubMed: 19194381]

61. Russo P, Catassi A, Cesario A, Servent D. Development of novel therapeutic strategies for lung cancer: targeting the cholinergic system. Curr Med Chem. 2006; 13:3493–3512. [PubMed: 17168719]

62. Paleari L, Sessa F, Catassi A, Servent D, Mourier G, et al. Inhibition of non-neuronal alpha7-nicotinic receptor reduces tumorigenicity in A549 NSCLC xenografts. Int J Cancer. 2009; 125:199211.

63. Catassi A, Paleari L, Servent D, Sessa F, Dominioni L, et al. Targeting alpha7-nicotinic receptor for the treatment of pleural mesothelioma. Eur J Cancer. 2008; 44:2296–2311. [PubMed: 18722110]

64. Paleari L, Negri E, Catassi A, Cilli M, Servent D, et al. Inhibition of nonneuronal alpha7-nicotinic receptor for lung cancer treatment. Am J Respir Crit Care Med. 2009; 179:1141–1150. [PubMed: 19151195]

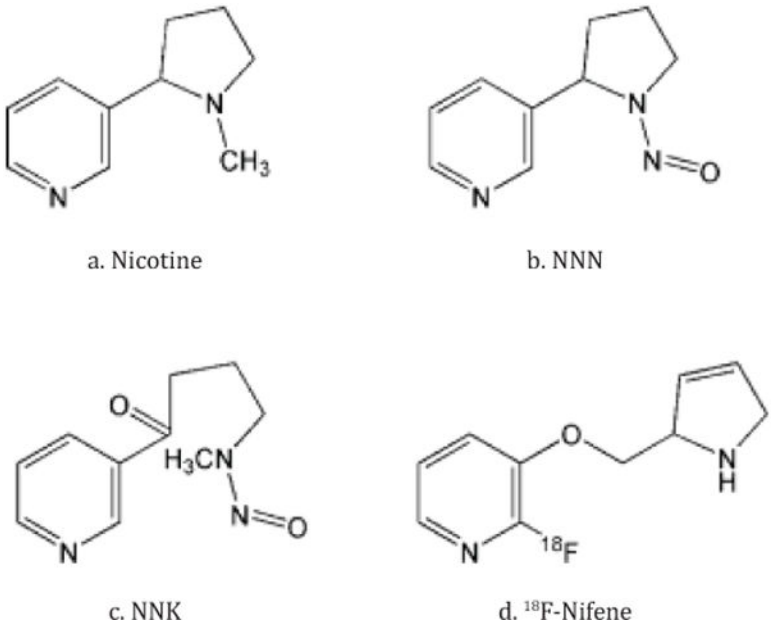

Figure 1.

Chemical structures of ^{18}F-Nifene and NNK. Structure of nicotine, its metabolites N′-nitrosonornicotine (NNN) and 4-(methylnitrosamino)-1-(3-pyridyl)-1-butanone (NNK), as well as ^{18}F-Nifene.

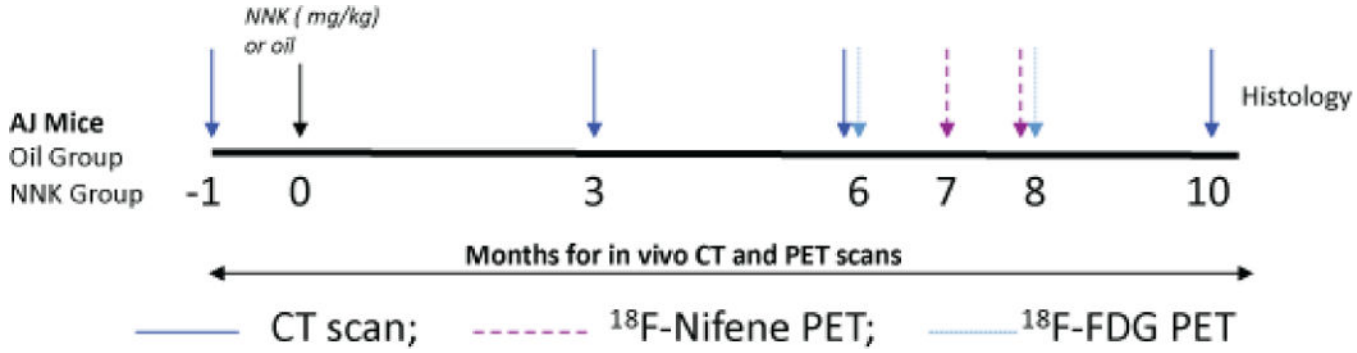

Figure 2.

Study time-line. Time-line of CT and PET scans of A/J mice injected with NNK vs. vehicle. CT scans were obtained on all mice at the baseline and 3, 6, and 10 months after treatment. ^{18}F-Nifene PET scans and ^{18}F-FDG PET scans were acquired on the month 8.

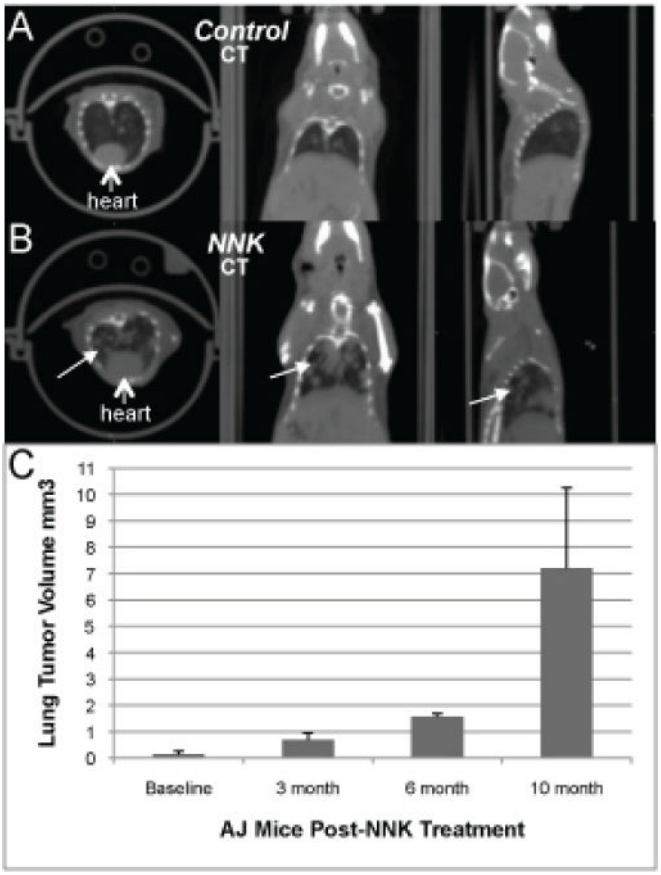

Figure 3.

CT Scans. Representative CT scans of (A) control and (B) NNK-treated AJ mice, showing lung tumors (arrows) 10 months after NNK treatment. (C) Time-course changes of the volumes of lung tumor growth in the NNK-treated AJ mice (data are mean ± SD, $p < 0.05$ for the different age groups). Baseline measures prior to NNK treatment indicating lung regions in the same animals were taken based on the contrast and may not necessarily reflect tumors.

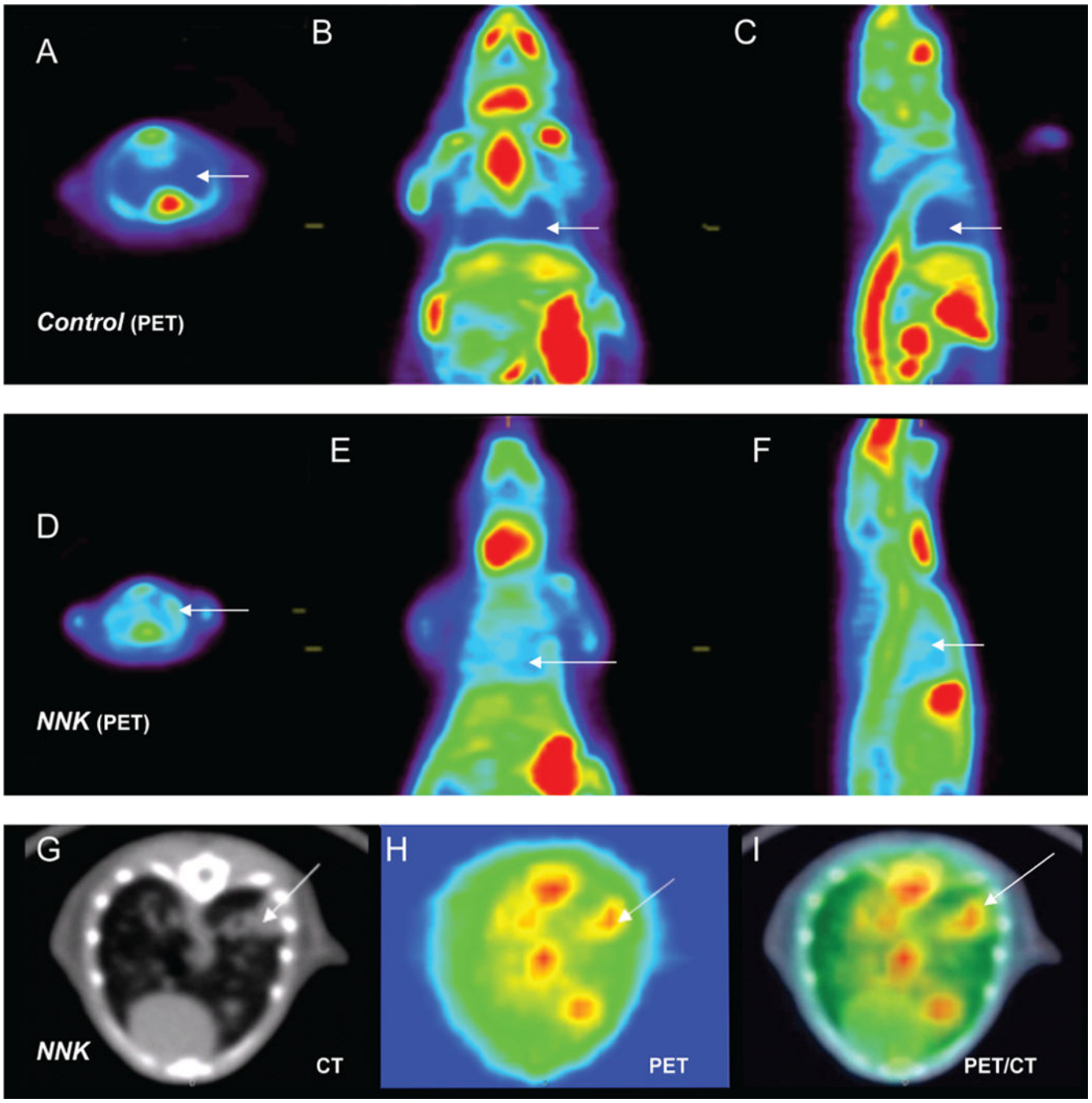

Figure 4.

^{18}F-Nifene PET/CT. Representative *in vivo* ^{18}F-Nifene PET images of control (A–C) and experimental A/J mice 8 months after NNK treatment (D–F). Arrows indicate reciprocal areas in the lungs in control and experiment mice. Transverse CT section (G), PET (H) and coregistered PET/CT image of NNK-treated mouse. Arrows indicate tumors identified by co-localization of ^{18}F-Nifene binding with CT images.

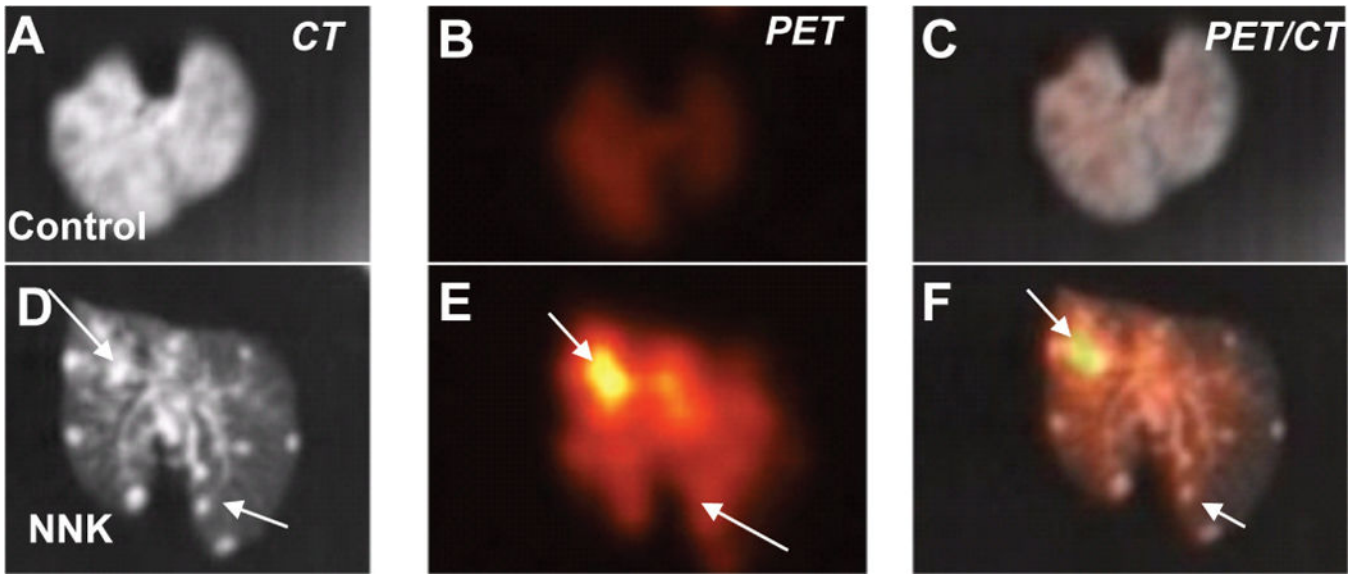

Figure 5. Ex vivo

^{18}F-Nifene PET/CT. Representative *ex vivo* ^{18}F-Nifene PET/CT images of A/J control mice (A–C) *vs.* mice treated with NNK (D–F). Arrows indicate lung tumors in CT image (D), PET image (E) and the coregistered CT/PET image (F). The images of the control mice (A–C) show significantly lower amount of ^{18}F-Nifene and the absence of tumors.

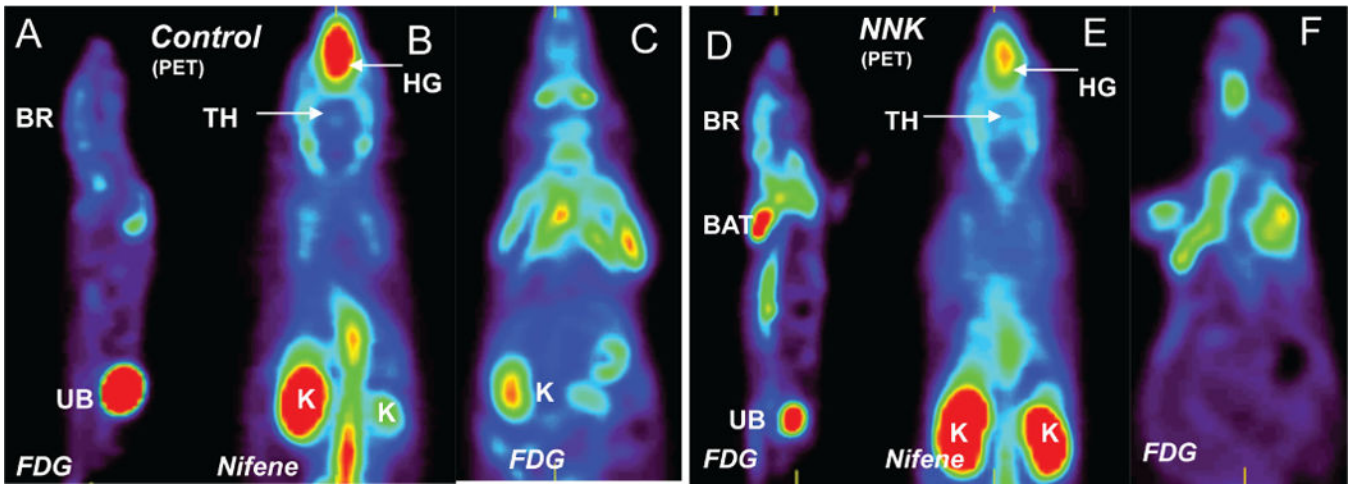

Figure 6.

Whole body ^{18}F-Nifene and ^{18}F-FDG imaging studies. Representative *in vivo* ^{18}F-FDG and ^{18}F-Nifene scans of control and NNK-treated A/J mice. (A) ^{18}F-FDG uptake in control mouse brain (BR) and excretion in the urinary bladder (UB). (B) ^{18}F-Nifene uptake in control mouse thalamus (TH) and excretion in kidneys (K). Nonspecific uptake was seen in the harderian glands (HG). (C) ^{18}F-FDG uptake in the coronal plane of the control mouse showing high activity in the upper chest and heart and kidneys (D) ^{18}F-FDG uptake in the NNK-treated mouse brain (BR), brown adipose tissue (BAT) and excretion in the urinary bladder (UB). (E) ^{18}F-Nifene uptake in the thalamus (TH) and excretion by kidneys (K) of the NNK-treated mouse. Nonspecific uptake was seen in the harderian glands (HG). (F) ^{18}F-FDG uptake in the coronal plane of the NNK mouse showing high activity in the upper chest and heart. Note: ^{18}F-FDG uptake is shown in the saggital plane to show the differences in brown adipose tissue binding, while ^{18}F-Nifene is selectively localized in the thalamus, brain and lungs.

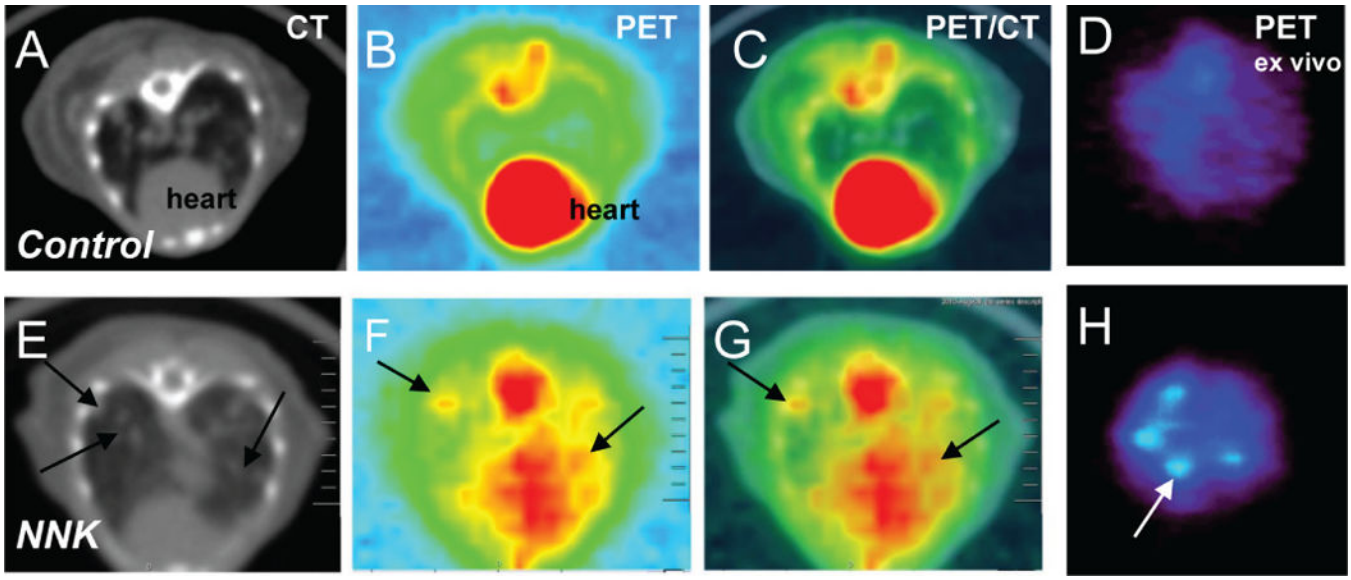

Figure 7.

^{18}F-FDG PET/CT. Representative transverse ^{18}F-FDG PET/CT images of control and NNK-treated mice. Designations are as in Figure 4C.

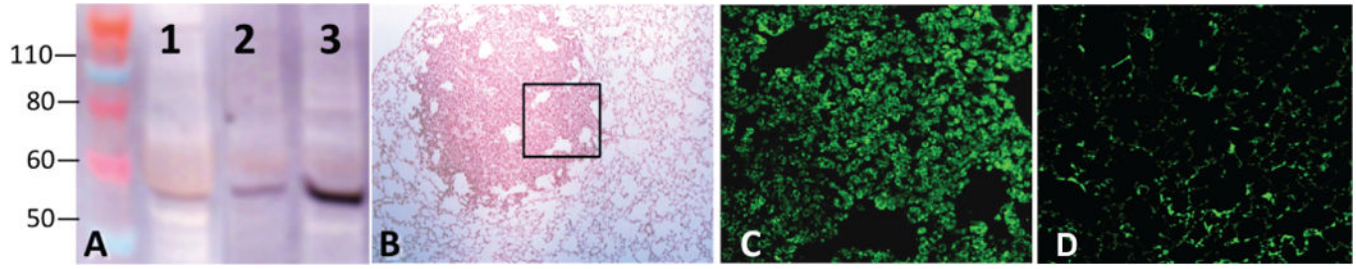

Figure 8.

Overexpression of α4 nAChR in lung tumors of A/J mice. (A) Immunoblots of lung proteins from tumor-free control mouse (1), and tumorfree (2) and tumor-containing (3) lungs of A/J mice treated with NNK (n = 4). The α4 protein band is seen at ~56 kD. (B) Light microscopy of lung tumor in A/J mouse. (C) Immunofluorescence staining for a4 in a serial lung section at the peripheral tumor area marked out in panel “B”. (D) Immunofluorescence staining for α4 in the lung of control mouse.

Table 1

Quantitation of CT and PET imaging in NNK-treated A/J mice

Study	*Baseline*	*3 months*	*6 months*	*8 months*	*10 months*	*Ex Vivo*
CT[A]	0.14 mm^3	0.70 mm^3	1.57 mm^3	na	7.2 mm^3	na
^{18}F-Nifene	na	na	na	1.8–2.0[b]	na	>4[d]
^{18}F-FDG	na	na	na	<1.5[c]	na	>3[e]

[a] *In vivo* measures of tumor volume in NNK-treated animals (n = 3, data are mean ± SD, $p < 0.05$ for the three age groups);

[b] Ratio of tumor/nontumor of ^{18}F-Nifene in NNK-treated animals;

[c] Ratio of tumor/nontumor of ^{18}F-FDG in NNK-treated animals;

[d] Ratio of tumor/nontumor of *ex vivo* lung ^{18}F-Nifene at 8 months post treatment;

[e] Ratio of Tumor/Nontumor of *ex vivo* lung ^{18}F-FDG at 8 months post treatment; na: not available.